A Computational Immune Approach for Modeling Different Levels of Severity in COVID-19 Infections

Laura Polverari e Silva[1 [0009−0004−2016−4093]] Marcelo Lobosco[1,2 [0000−0002−7205−9509]] and Ruy Freitas Reis[1,2⋆ [0000−0001−5215−3744]]

[1] Departamento de Ciência da Computação, Universidade Federal de Juiz de Fora, Brazil
[2] Pós-Graduação em Modelagem Computacional, Universidade Federal de Juiz de Fora, Brazil
ruy.reis@ufjf.br

Abstract. This study introduces a computational model designed to simulate the human immune response to SARS-CoV-2, validated against data from multiple clinical studies. The model captures the temporal dynamics of mature $CD4^+$ T cells, mature $CD8^+$ T cells, viral load, and antibody levels across three COVID-19 severity profiles: mild, severe, and critical. In all simulated scenarios, the model-generated trajectories remained primarily within the confidence intervals of empirical data, demonstrating its capacity to qualitatively reproduce key trends in immune responses across varying disease severities.

Keywords: Computational Immunology · COVID-19 · SARS-CoV-2 · Differential Evolution · Optimization

1 Introduction

COVID-19 is caused by SARS-CoV-2, first identified in Wuhan, China, in December 2019 [6]. Following its global spread, the WHO declared a pandemic on March 11, 2020 [6]. As of February 2025, the disease has resulted in over 777 million cases and 7 million deaths worldwide [6], alongside significant economic and societal disruptions [1].

Mathematical models have been widely used to understand COVID-19 pathogenesis. A notable model by Reis *et al.* [4] employed 15 ODEs to simulate viral and immune dynamics but only validated a subset of its equations against cohort data. Zhang *et al.* [8] analyzed immune responses by disease severity, offering insights into $CD4^+$ and $CD8^+$ T cells and cytokines. Xavier *et al.* [7] validated a reduced model using ChAdOx1 nCoV-19 vaccine data.

This study adapts the previously proposed model [4] to simulate disease severity (mild, severe, critical) by calibrating it with differential evolution and validating it against data on $CD4^+$ and $CD8^+$ T cells, viral load, and antibodies following symptom onset.

⋆ corresponding author

ICCS Camera Ready Version 2025
To cite this paper please use the final published version:
DOI: 10.1007/978-3-031-97554-7_28

2 Methods

2.1 Mathematical Model

The model consists of twelve ordinary differential equations (ODEs) representing key components of the immune response to SARS-CoV-2 infection. The first equation (Eq. (1)) describes viral dynamics (V). The virus replicates at rate π_v, is eliminated by the innate immune system at a saturable rate $\frac{c_{v1}V}{c_{v2}+V}$ [3], and by the adaptive immune system via antibody binding ($k_{v1}VA$) and CD8$^+$ T cell action ($k_{v2}VT_{ke}$).

$$\frac{d}{dt}V = \pi_v V - \frac{c_{v1}V}{c_{v2}+V} - k_{v1}VA - k_{v2}VT_{ke}. \tag{1}$$

Immature antigen-presenting cells (APCs, A_p) follow Eq.(2), maintained through homeostasis and activated in response to viral load. These activated cells (A_{pm}), governed by Eq.(3), decay at rate δ_{apm}.

$$\frac{d}{dt}A_p = \alpha_{ap}(A_{p0} - A_p) - \beta_{ap}A_p\frac{c_{ap1}V}{c_{ap2}+V} \tag{2}$$

$$\frac{d}{dt}A_{pm} = \beta_{ap}A_p\frac{c_{ap1}V}{c_{ap2}+V} - \delta_{apm}A_{pm} \tag{3}$$

Eqs. (4) and (5) describe naïve (T_{hn}) and effector (T_{he}) CD4$^+$ T cells. Homeostasis and activation are modeled for T_{hn}, while T_{he} dynamics include activation, proliferation, and decay.

$$\frac{d}{dt}T_{hn} = \alpha_{th}(T_{hn0} - T_{hn}) - \beta_{th}A_{pm}T_{hn} \tag{4}$$

$$\frac{d}{dt}T_{he} = \beta_{th}A_{pm}T_{hn} + \pi_{th}A_{pm}T_{he} - \delta_{th}T_{he} \tag{5}$$

Eqs. (6) and (7) represent naïve (T_{kn}) and effector (T_{ke}) CD8$^+$ T cells, including homeostatic maintenance, activation, proliferation, and decay processes.

$$\frac{d}{dt}T_{kn} = \alpha_{tk}(T_{kn0} - T_{kn}) - \beta_{tk}A_{pm}T_{kn} \tag{6}$$

$$\frac{d}{dt}T_{ke} = \beta_{tk}A_{pm}T_{kn} + \pi_{tk}A_{pm}T_{ke} - \delta_{tk}T_{ke} \tag{7}$$

Eq. (8) models B cell dynamics (B), incorporating homeostasis and proliferation via T-independent and T-dependent mechanisms. Differentiation into plasma and memory B cells occurs via interactions with APCs and CD4$^+$ T cells.

$$\frac{d}{dt}B = \alpha_b(B_0 - B) + \pi_{b1}VB + \pi_{b2}T_{he}B - \beta_{ps}A_{pm}B - \beta_{pl}T_{he}B - \beta_{bm}T_{he}B \tag{8}$$

ICCS Camera Ready Version 2025
To cite this paper please use the final published version:
DOI: 10.1007/978-3-031-97554-7_28

Short- and long-lived plasma cells are modeled in Eqs. (9) and (10), respectively. Both arise from B cell differentiation and decay naturally; long-lived plasma cells also receive contributions from memory B cells.

$$\frac{d}{dt}P_s = \beta_{ps}A_{pm}B - \delta_{ps}P_s \tag{9}$$

$$\frac{d}{dt}P_l = \beta_{pl}T_{he}B - \delta_{pl}P_l + \gamma_{bm}B_m \tag{10}$$

Memory B cells (B_m), governed by Eq. (11), form through differentiation and expand via logistic growth. They can also revert to long-lived plasma cells.

$$\frac{d}{dt}B_m = \beta_{bm}T_{he}B + \pi_{bm1}B_m\left(1 - \frac{B_m}{\pi_{bm2}}\right) - \gamma_{bm}B_m \tag{11}$$

Finally, Eq. (12) represents antibody production (A), which depends on the activity of both short- and long-lived plasma cells and includes a decay term.

$$\frac{d}{dt}A = \pi_{ps}P_s + \pi_{pl}P_l - \delta_a A \tag{12}$$

More details about these equations can be obtained in the original work of Reis *et al.* [4].

2.2 Differential Evolution

In this work, Differential Evolution (DE) [5] is applied to optimize a set of parameters p so that the model's numerical results best fit experimental data describing the populations of mature CD4$^+$ T cells, CD8$^+$ T cells, viruses, and antibodies.

The objective function, defined in Eq. (13), quantifies the weighted relative error between simulated outputs ($\overline{T_{he}}$, $\overline{T_{ke}}$, $\overline{V}$, $\overline{A}$) and experimental data (T_{he}, T_{ke}, V, A):

$$\min\ O(p) = \omega_{T_{he}}\frac{\|T_{he} - \overline{T_{he}}\|_2}{\|T_{he}\|_2} + \omega_{T_{ke}}\frac{\|T_{ke} - \overline{T_{ke}}\|_2}{\|T_{ke}\|_2} + \omega_V\frac{\|V - \overline{V}\|_2}{\|V\|_2} + \omega_A\frac{\|A - \overline{A}\|_2}{\|A\|_2}, \tag{13}$$

Additionally, each ω_* represents the weight assigned to the error associated with each of these populations (T_{he}, T_{ke}, V, and A).

3 Numerical Results

The mathematical model was implemented in C++ using the CVODE package to solve systems of ordinary differential equations. CVODE integrated the ODE system using the Backward Differentiation Formula (BDF) [2]. Additionally, a library implementing the DE algorithm was utilized [3]. GCC (*GNU Compiler*

[3] `https://github.com/ruyfreis/differential_evolution.git`

ICCS Camera Ready Version 2025
To cite this paper please use the final published version:
DOI: 10.1007/978-3-031-97554-7_28

Collection) version 13.2.0 compiled the source code. The model results' graphs were produced using the `Python 3.12.3` and the `Matplotlib` library.

Three clinical scenarios—mild, severe, and critical—are considered for simulations, based on $CD4^+$ and $CD8^+$ T cell population data from the literature [8]. Each scenario uses distinct lymphocyte data, while virus concentration and antibody levels come from a single shared dataset. Table 2 presents the initial conditions and parameter values used in each scenario and the parameters optimized via DE and their bounds. In addition to the values available in the tables, we consider, for all cases, parameters $c_{v1} = 1.1258 \times 10^{-9}$, $c_{v2} = 6.0 \times 10^{-1}$, $\alpha_{th} = 2.17 \times 10^{-1}$, $\alpha_b = 3.58 \times 10^2$, $\pi_{b1} = 8.98 \times 10^{-5}$, $\pi_{b2} = 1.27 \times 10^{-8}$, $\beta_{ps} = 6.0 \times 10^{-6}$, $\beta_{pl} = 5.0 \times 10^{-6}$, $\beta_{bm} = 1.0 \times 10^{-6}$, $\delta_{ps} = 2.5$, $\delta_{pl} = 3.5 \times 10^{-1}$, $\gamma_{bm} = 9.75 \times 10^{-4}$, π_{bm1} 8.1117, $\pi_{bm2} = 3.7965 \times 10^3$, and $\pi_{ps} = 4.0041 \times 10^4$. Moreover, for the initial conditions, we consider $A_{p0} = 1.0 \times 10^6$, $A_{pm0} = 0.0$, $T_{hn0} = 1.0 \times 10^6$, $T_{he0} = 0.0$, $T_{kn0} = 5.0 \times 10^5$, $T_{ke0} = 0.0$, $B_0 = 2.5 \times 10^5$, $P_{s0} = 0.0$, $P_{l0} = 0.0$, $B_{m0} = 0.0$, $A_0 = 0.0$, and Tab. 2 shows V_0 for each scenario.

Model results for $CD4^+$ and $CD8^+$ T cells, viruses, and antibodies are plotted alongside literature data. Virus and antibody levels are shown on $\log_{10}$ and $\log_2$ scales, respectively. Literature data reflect measurements taken after hospitalization; thus, data points do not align with simulation day zero. Orange dots represent medians (or means for the virus), with bars denoting confidence intervals or standard deviations. In all scenarios, Eq. (13) uses weights $\omega_{T_{he}} = 0.26$, $\omega_{T_{ke}} = 0.38$, $\omega_V = 0.23$, and $\omega_A = 0.13$, normalized to sum to 1.

3.1 Experiments

This section presents the results of parameter adjustments for the mild, severe, and critical scenarios using DE. Tab. 1 shows the parameters and bounds used in each case. For the mild and severe cases, 15 parameters (14 model parameters and one initial condition) are optimized; for the critical case, 12 parameters (11 model parameters and one initial condition) are adjusted.

In the mild scenario, 14 parameters and the initial virus load V_0 are optimized. Tab. 1 provides parameter bounds, while Tab. 2 lists the initial condition value and parameters the optimization determines. Model results are shown in Fig. 1: virus (A), antibodies (B), $CD4^+$ T cells (C), and $CD8^+$ T cells (D). The same optimization strategy is applied to 14 parameters and V_0 in the severe case. Tabs 1 and 2 contain bounds, initial conditions, and final parameter values, respectively. Results are displayed in Fig. 2: virus (A), antibodies (B), $CD4^+$ T cells (C), and $CD8^+$ T cells (D).

The critical case involves optimizing 11 parameters and V_0. Tab. 1 shows parameter limits; Tab. 2 lists initial conditions and the parameter values. Simulation outcomes are shown in Fig. 3: virus (A), antibodies (B), $CD4^+$ T cells (C), and $CD8^+$ T cells (D).

The simulation results align well with the literature and offer insights into immune dynamics in mild, severe, and critical scenarios. Within each case, comparisons of population behavior reveal the interplay between immune response

ICCS Camera Ready Version 2025
To cite this paper please use the final published version:
DOI: 10.1007/978-3-031-97554-7_28

Table 1. DE optimization bounds: minimum and maximum search space constraints.

Parameter	Bounds		
	Mild	**Severe**	**Critical**
V_0	$[5.7 \times 10^4, 1.1 \times 10^6]$	$[1.1 \times 10^5, 2.1 \times 10^6]$	$[6.6 \times 10^5, 1.2 \times 10^7]$
π_v	$[1.5 \times 10^{-2}, 2.9 \times 10^{-1}]$	$[9.6 \times 10^{-3}, 1.8 \times 10^{-1}]$	$[1.6 \times 10^{-4}, 3.0 \times 10^{-3}]$
β_{tk}	$[8.9 \times 10^0, 1.7 \times 10^2]$	$[6.1 \times 10^0, 1.2 \times 10^2]$	$[3.1 \times 10^0, 5.9 \times 10^1]$
c_{ap1}	-	$[8.0 \times 10^{-2}, 1.5 \times 10^0]$	-
k_{v1}	$[8.9 \times 10^{-8}, 1.7 \times 10^{-6}]$	-	-
k_{v2}	$[9.0 \times 10^{-8}, 1.8 \times 10^{-6}]$	$[5.1 \times 10^{-8}, 9.7 \times 10^{-7}]$	$[6.1 \times 10^{-7}, 1.2 \times 10^{-5}]$
β_{ap}	$[7.7 \times 10^3, 1.5 \times 10^5]$	$[8.7 \times 10^3, 1.7 \times 10^5]$	$[7.9 \times 10^4, 1.5 \times 10^6]$
δ_{apm}	$[3.1 \times 10^7, 6.0 \times 10^8]$	$[1.0 \times 10^7, 1.9 \times 10^8]$	$[1.1 \times 10^7, 2.1 \times 10^8]$
π_{tk}	$[3.4 \times 10^0, 6.7 \times 10^1]$	$[6.2 \times 10^{-1}, 1.2 \times 10^1]$	$[4.7 \times 10^{-2}, 8.9 \times 10^{-1}]$
δ_{tk}	$[5.5 \times 10^{-3}, 1.1 \times 10^{-1}]$	$[2.3 \times 10^{-3}, 4.3 \times 10^{-2}]$	$[2.4 \times 10^{-4}, 4.7 \times 10^{-3}]$
π_{pl}	$[1.4 \times 10^2, 2.9 \times 10^3]$	-	-
c_{ap2}	-	$[1.6 \times 10^6, 3.1 \times 10^7]$	-
δ_a	$[1.1 \times 10^7, 2.2 \times 10^8]$	$[1.1 \times 10^7, 2.1 \times 10^8]$	$[3.8 \times 10^7, 7.2 \times 10^8]$
α_{tk}	$[6.2 \times 10^{-3}, 1.2 \times 10^{-1}]$	$[9.1 \times 10^{-4}, 1.7 \times 10^{-2}]$	$[3.6 \times 10^2, 6.8 \times 10^3]$
β_{th}	$[8.4 \times 10^0, 1.7 \times 10^2]$	$[2.3 \times 10^0, 4.3 \times 10^1]$	-
π_{th}	$[1.1 \times 10^1, 2.3 \times 10^2]$	$[2.4 \times 10^0, 4.5 \times 10^1]$	$[9.9 \times 10^{-1}, 1.9 \times 10^1]$
δ_{th}	$[1.5 \times 10^{-2}, 3.0 \times 10^{-1}]$	$[4.1 \times 10^{-3}, 7.8 \times 10^{-2}]$	$[7.9 \times 10^{-3}, 1.5 \times 10^{-1}]$

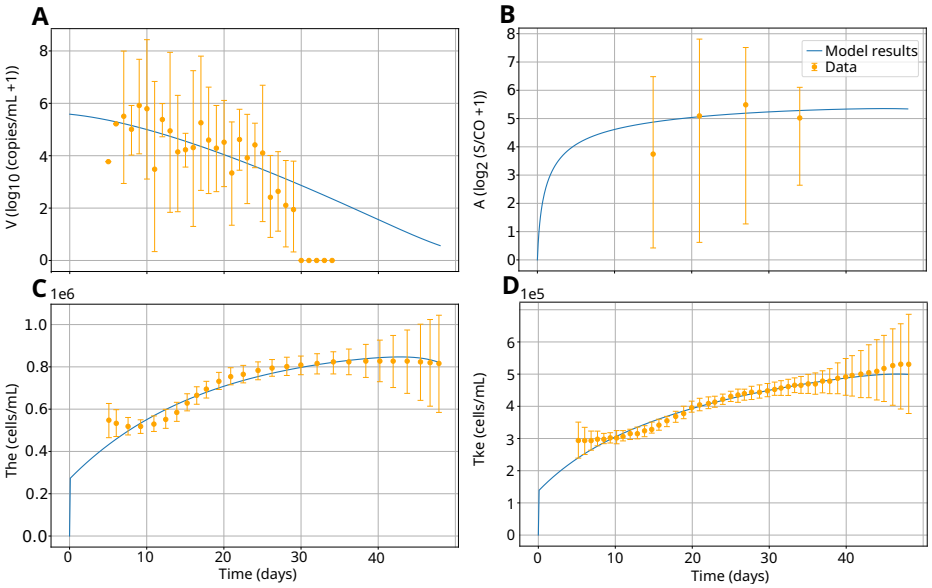

Fig. 1. Results for the mild case of V, A, T_{he}, and T_{ke} population over time.

and disease progression. Cross-scenario comparisons highlight how disease severity affects these dynamics. In all scenarios, mature $CD4^+$ T cell concentrations

ICCS Camera Ready Version 2025
To cite this paper please use the final published version:
DOI: 10.1007/978-3-031-97554-7_28

Table 2. Optimized ODE parameters and initial condition for all cases.

Parameter	Value			Unit
	Mild	Severe	Critical	
π_v	2.8683×10^{-2}	1.6895×10^{-2}	5.7001×10^{-4}	(day^{-1})
k_{v1}	9.2652×10^{-7}	8.9368×10^{-7}	8.9368×10^{-5}	$(\text{day}^{-1}\ \frac{\text{mL}}{\text{S/CO}})$
k_{v2}	7.0636×10^{-7}	7.5329×10^{-7}	1.1651×10^{-6}	$(\text{day}^{-1}\ \frac{\text{mL}}{\text{cells}})$
α_{ap}	2.5999×10^{-1}	1.0373×10^{-1}	5.1378×10^{-1}	$(\text{day}^{-1}\ \frac{\text{mL}}{\text{pg}})$
β_{ap}	1.0259×10^{5}	1.2021×10^{5}	1.3548×10^{6}	$(\text{day}^{-1}\ \frac{\text{mL}}{\text{copies}})$
c_{ap1}	4.0826×10^{0}	1.1797×10^{-1}	7.2874×10^{0}	(copies/mL)
c_{ap2}	4.8549×10^{5}	1.8840×10^{7}	9.2035×10^{6}	(copies/mL)
δ_{apm}	4.2412×10^{8}	8.4049×10^{7}	1.8347×10^{8}	(day^{-1})
β_{th}	1.1144×10^{2}	1.6255×10^{1}	7.6477×10^{0}	$(\text{day}^{-1}\ \frac{\text{mL}}{\text{cells}})$
π_{th}	1.2320×10^{2}	4.3853×10^{1}	1.8671×10^{1}	$(\text{day}^{-1}\ \frac{\text{mL}}{\text{cells}})$
δ_{th}	1.3234×10^{-1}	6.3894×10^{-2}	1.0954×10^{-1}	(day^{-1})
α_{tk}	7.5835×10^{-2}	1.2081×10^{-2}	4.8726×10^{2}	$(\text{day}^{-1}\ \frac{\text{mL}}{\text{pg}})$
β_{tk}	1.3030×10^{2}	5.0688×10^{1}	3.4262×10^{0}	$(\text{day}^{-1}\ \frac{\text{mL}^2}{\text{pg cells}})$
π_{tk}	2.7494×10^{1}	3.8017×10^{0}	6.7469×10^{-2}	$(\text{day}^{-1}\ \frac{\text{mL}}{\text{cells}})$
δ_{tk}	4.9948×10^{-2}	2.3070×10^{-2}	4.1096×10^{-3}	(day^{-1})
π_{pl}	2.5121×10^{3}	2.0041×10^{3}	1.4197×10^{4}	$(\text{day}^{-1}\ \frac{\text{mL}}{\text{cells}\cdot(\text{S/CO})})$
δ_a	1.8720×10^{8}	1.0543×10^{8}	3.8668×10^{8}	(day^{-1})
V_0	3.8447×10^{5}	1.6366×10^{6}	7.2274×10^{5}	(copies/mL)

exceed $CD8^+$ levels throughout the simulation, suggesting stronger $CD4^+$ proliferation during infection. Antibody levels increase rapidly, peak, and stabilize, while virus levels decline as immune components rise, reflecting typical immune responses. In the mild case, T cell levels increase sharply until day 30, coinciding with a significant drop in virus concentration. So, it suggests efficient viral clearance due to sufficient lymphocyte presence. In the severe case, both T cell types peak around day 30, then decline, with virus levels dropping more slowly than in the mild case—likely due to the reduced lymphocyte counts post-peak. The critical case shows only modest T cell increases and delayed viral decline, with significant reduction occurring after T cell levels peak between days 30 and 60. Overall, milder cases show higher T cell levels and faster viral clearance, while critical cases display reduced immune response and prolonged viral presence, indicating a severity-linked immune dysfunction.

4 Conclusions and Future Works

This study presented a computational model for simulating the immune response to SARS-CoV-2, validated using experimental data across mild, severe, and criti-

ICCS Camera Ready Version 2025
To cite this paper please use the final published version:
DOI: 10.1007/978-3-031-97554-7_28

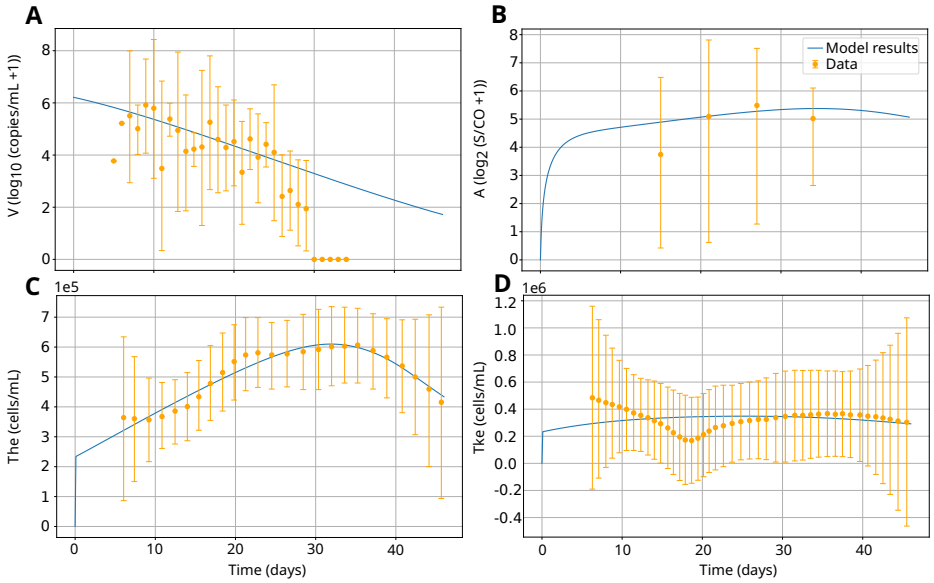

Fig. 2. Results for the severe case of V, A, T_{he}, and T_{ke} population over time.

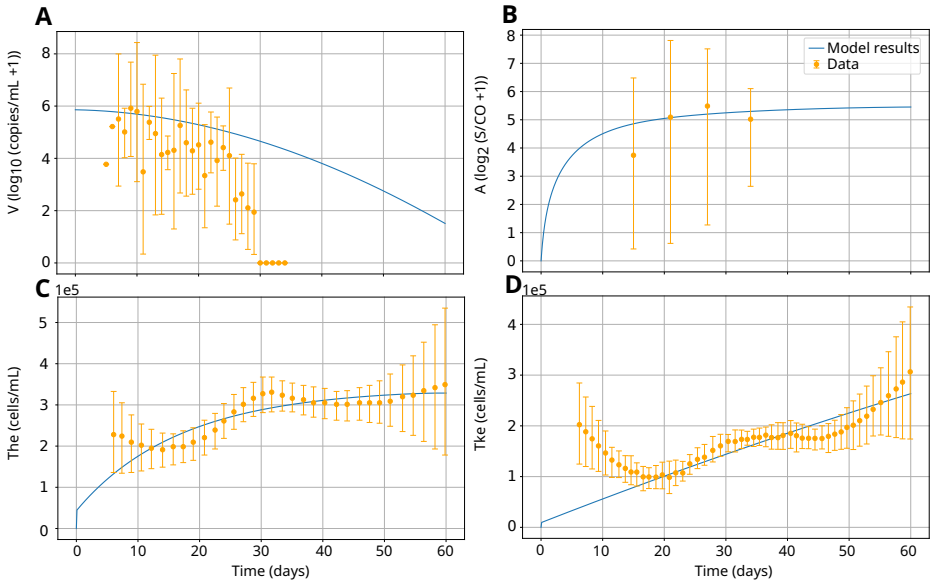

Fig. 3. Results for the critical case of V, A, T_{he}, and T_{ke} population over time.

cal cases. Using a consistent dataset, the model captured the dynamics of mature $CD4^+$ and $CD8^+$ T cells, viruses, and antibodies. In the mild case, all population trends closely matched the data. For the severe case, $CD4^+$ T cells, viruses,

ICCS Camera Ready Version 2025
To cite this paper please use the final published version:
DOI: 10.1007/978-3-031-97554-7_28

and antibodies aligned well, though $CD8^+$ T cells showed early-stage discrepancies. In the critical case, model predictions were most accurate for $CD4^+$ T cells and antibodies but diverged notably for $CD8^+$ T cells and viruses. Despite some deviations, the simulated curves generally remained within the experimental confidence intervals, demonstrating the model's qualitative validity.

Future work will incorporate uncertainty quantification, sensitivity analysis, and high-performance computing to better understand and reduce discrepancies, as well as to improve the model's accuracy and efficiency.

Acknowledgments. This work has been supported by UFJF, by CAPES - Finance Code 001; by CNPq - Grant number 308745/2021-3; by FAPEMIG Grant number APQ-02513-22; and by FINEP SOS Equipamentos 2021 AV02 0062/22.

Disclosure of Interests. The authors have no competing interests to declare that are relevant to the content of this article.

References

1. Barai, M.K., Dhar, S.: Covid-19 pandemic: Inflicted costs and some emerging global issues. Global Business Review **25**(3), 812–831 (Mar 2021)
2. Gardner, D.J., Reynolds, D.R., Woodward, C.S., Balos, C.J.: Enabling new flexibility in the SUNDIALS suite of nonlinear and differential/algebraic equation solvers. ACM Transactions on Mathematical Software (TOMS) **48**(3), 1–24 (2022)
3. Goutelle, S., Maurin, M., Rougier, F., Barbaut, X., Bourguignon, L., Ducher, M., Maire, P.: The hill equation: a review of its capabilities in pharmacological modelling. Fundamental & Clinical Pharmacology **22**(6), 633–648 (Nov 2008)
4. Reis, R., Pigozzo, A., Bonin, C., Quintela, B.d.M., Pompei, L., Vieira, A., Silva, L.L., Xavier, M.P., Weber dos Santos, R., Lobosco, M.: A validated mathematical model of the cytokine release syndrome in severe COVID-19. Front. Molecular Biosci. **8** (2021)
5. Storn, R., Price, K.: Differential evolution – a simple and efficient heuristic for global optimization over continuous spaces. Journal of Global Optimization **11**(4), 341–359 (1997)
6. WHO: Coronavirus disease (covid-19) pandemic. Available at: `https://www.who.int/europe/emergencies/situations/covid-19` (2023), accessed on February 05, 2025
7. Xavier, M.P., Pompei, L.T., de O. Vieira, A.C.G., de Paula, M.A.M., Bonin, C.R.B., Reis, R.F., Pigozzo, A.B., Quintela, B.d.M., Dos Santos, R.W., Lobosco, M.: Modelling the human immune system response to the chadox1 ncov-19 vaccine. In: 2021 IEEE International Conference on Bioinformatics and Biomedicine (BIBM). p. 3327–3333. IEEE (Dec 2021)
8. Zhang, X., Tan, Y., Ling, Y., Lu, G., Liu, F., Yi, Z., Jia, X., Wu, M., Shi, B., Xu, S., Chen, J., Wang, W., Chen, B., Jiang, L., Yu, S., Lu, J., Wang, J., Xu, M., Yuan, Z., Zhang, Q., Zhang, X., Zhao, G., Wang, S., Chen, S., Lu, H.: Viral and host factors related to the clinical outcome of covid-19. Nature **583**(7816), 437–440 (May 2020)

ICCS Camera Ready Version 2025
To cite this paper please use the final published version:
DOI: 10.1007/978-3-031-97554-7_28